Journal of Photochemistry and Photobiology A: Chemistry 212 (2010) 135–141

Contents lists available at ScienceDirect

Journal of Photochemistry and Photobiology A: Chemistry

journal homepage: www.elsevier.com/locate/jphotochem

Enhancement of TiO_2 visible light photoactivity through accumulation of defects during reduction–oxidation treatment

Igor N. Martyanov[a,*], Thomas Berger[b], Oliver Diwald[b], Shalini Rodrigues[a], Kenneth J. Klabunde[a]

[a] Department of Chemistry, Kansas State University, Manhattan, KS 66506, United States
[b] Institut für Materialchemie, Technical University of Vienna, A-1210 Vienna, Austria

ARTICLE INFO

Article history:
Received 2 January 2010
Received in revised form 31 March 2010
Accepted 7 April 2010
Available online 14 April 2010

Keywords:
Photocatalyst
TiO_2
Visible light
Magnelli
Ti_nO_{2n-1}
Raman

ABSTRACT

Rutile-TiO_2, obtained by treatment of Degussa P25 at $T = 800\,^{\circ}C$ in oxygen, is used as a starting material and initially shows only marginal optical absorption and photocatalytic activity in the visible range. Treatment at temperatures $T \geq 1000\,^{\circ}C$ in a hydrogen atmosphere leads to the phase transformation: rutile-$TiO_2 \rightarrow Ti_nO_{2n-1}$ ($n < 9$). Subsequent treatment at $T = 800\,^{\circ}C$ in oxygen restores the initial rutile structure. The reduction–reoxidation cycle, however, induces a growth of an optical absorption in the visible range, which is accompanied by a substantial increase of TiO_2 powders photoactivity in the reaction of acetaldehyde oxidation under visible light ($\lambda = 546$ nm, $T = 298$ K). In order to characterize the nature of the respective defect sites, charge carrier trapping has been followed by EPR technique. At $T = 77$ K under high vacuum conditions ($p < 10^{-6}$ mbar), paramagnetic $O^{\bullet -}$ centers (trapped holes) and Ti^{3+} centers (trapped electrons) are observed after supra-band-gap excitation ($200\text{ nm} < \lambda < 387$ nm) on both the visible-light-inactive and the visible-light-active samples. Visible light ($\lambda > 495$ nm) illumination results in formation of $O^{\bullet -}$ and Ti^{3+} centers exclusively in visible-light-active samples, which is in line with the photocatalytic activity tests. An analysis of Raman spectroscopy data indicates that the reduction–reoxidation cycle results in introduction of oxygen defects in the TiO_2 lattice. A possible contribution of other structural defects to the appearance of visible light activity in TiO_2 is discussed.

1. Introduction

Sparked by publication by Fujishima and Honda [1], heterogeneous photocatalytic processes have continued to attract attention of scientific and business communities. Numerous photocatalytic visible-light-active materials have been discovered in the last decade. New formulations with photocatalytic properties: CrO_x [2], CoO_x [3], AgBr [4,5] were shown to become photoactive as particle sizes approach a nanometer range; isolated ions of Cr^{6+} [6,7], V^{5+} [8] in silica matrix as well as $CaIn_2O_4$ [9], $In_{1-x}Ni_xTaO_4$ [10] and other compositions [11,12] have also exhibited photoactivities under visible light.

A great deal of research is still focused on the properties and phenomena occurring over TiO_2. Indeed, low toxicity, low cost and the high stability of titanium dioxide even in harsh environment of radical oxidation processes make this material quite attractive for practical applications. On the surface of illuminated TiO_2, oxidation of many toxic organic substances can proceed at a reasonably high speed in the presence of atmospheric concentrations of oxygen at room temperature and below. The regularities of the photooxidation processes over TiO_2 have been extensively reviewed in the literature [13–20].

One limitation hindering practical use of TiO_2-based photocatalytic processes is a necessity of the UV irradiation. A number of strategies to overcome this obstacle have been suggested. Among them, doping TiO_2-based materials with various transition metals [12,21,22] and non-metals remain the most studied.

Only relatively recently, the finding by Sato [23] on visible-light-active N-doped TiO_2 has received its due attention [24–28]. Later, the incorporation of the other non-metal elements, such as C [29–32], S [33–35], B [36] or even I [37] were found to induce a similar effect leading to an intensive discussion in regard to the nature of this intriguing phenomenon [38–41]. Valentin et al. [40,41] investigated various structural models of nitrogen and carbon impurities in TiO_2 by means of quantum-chemical calculations. They found that impurities result only in modest variations of the bandgap but instead induce several localized occupied states in it [42]. Except for very oxidizing atmospheres, nitrogen is generally found in substitutional (to oxygen) positions and stabilized by the presence of oxygen vacancies. Carbon on the other hand exhibits a more complex chemistry when introduced into TiO_2. For low carbon concentrations substitutional (to oxygen) carbon and oxygen vacancies are favored in a reducing environment, whereas interstitial and substitutional (to Ti) C atoms are preferred in an oxidizing

* Corresponding author.
E-mail address: Igor_Martyanov@hotmail.com (I.N. Martyanov).

1010-6030/$ – see front matter © 2010 Elsevier B.V. All rights reserved.
doi:10.1016/j.jphotochem.2010.04.006

atmosphere. The authors speculated that the origin of the increased photoactivity of C and N-doped TiO_2 could be associated with more complex phenomena than a simple presence of the impurity atoms, for example, concomitant changes in the stoichiometry.

Ihara et al. [43,44] reported a change in the color of anatase TiO_2 powders after hydrogen plasma treatment from white to yellow, which was attributed to the substoichiometry of the resulting material. Furthermore, a visible light activity for NO removal at 298 K was observed and a linear correlation of the NO removal percentage and the EPR signal at $g = 2.003$, measured after irradiation at 77 K under inert gas, was revealed. The authors speculated that both, the visible light photocatalytic activity as well as the EPR signal result from the formation of oxygen vacancy states in the course of the plasma treatment.

Some time ago we reported that an oxidative annealing of titanium oxides Ti_2O_3 or TiO leads to the rutile-TiO_2 with visible light activities exceeding the activity of titanium dioxide analogously prepared from TiN [45]. With the idea in mind that reoxidation of titanium oxides with titanium in a low oxidation state could be a key step in the formation of a dopant-free visible-light-active TiO_2, the present study on the properties of titanium dioxide prepared from various suboxides Ti_nO_{2n-1} has been undertaken.

2. Experimental

2.1. Reagents and materials

TiO_2 P25 from Degussa Company, acetaldehyde from Aldrich, oxygen from Airgas and 4% (v/v) of hydrogen in argon from Linweld were used as-received.

2.2. Preparation of the catalysts

The oxidation–reduction–oxidation cycles in preparation of TiO_2 were cycle of TiO_2 was carried out in a tube furnace from Carbolite Company under continuous 20 mL/min flow of appropriate gases. First to burn the residual organic compounds, about 2 g of the original TiO_2 Degussa P25 in a quartz boat was subjected to oxidation in the flow of oxygen according to the program: ramp 1°/min from room temperature to 800 °C, hold at 800 °C for 2 h, ramp back to room temperature at 1°/min. The second step was a reduction of the pretreated TiO_2 in the flow of 4 volume percent of H_2 in Ar conducted according to the temperature program: 1°/min ramp from room temperature to a desired temperature (1000, 1100, or 1180 °C), a hold at that temperature for 2 h followed by cooling to room temperature at 1 °/min. The third reoxidation step was a repetition of the first oxidation. The sample subjected only to the first oxidation step was designated as sample A, whereas the samples prepared through oxidation–reduction–oxidation cycle were labeled as sample B, sample C, and sample D, respectively.

2.3. Characterization of the catalysts

All XRD patterns were recorded under atmospheric conditions on a Bruker AXS D8 X-ray diffractometer equipped with Cu Kα source and operating in 0.02° step mode with 1 s/step acquisition time. The phase analysis of the samples was done through comparison of recorded XRD patterns with the diffractometer database.

Optical absorption spectra of the powders were recorded on a Cary 500 Scan UV-Vis-NIR spectrophotometer from Varian Analytical Instruments equipped with a Diffuse Reflectance Accessory. Polytetrafluoroethylene powder was used as a reference standard in each case. All spectra were recorded at 600 nm/min scan rate with 5 nm slit resolution.

Raman spectra were recorded on Nexus 670 FTIR Spectrometer with an attached FT-Raman Module from Nicolet Company. The position of the laser beam ($\lambda = 1024$ nm) was adjusted to achieve maximum signal intensity at 2 cm^{-1} resolution. The recorded spectra were an average of 1024 scans.

The visible light photoactivities of samples A–D were later examined in the reaction of gaseous acetaldehyde oxidation. In a typical test, about 100 mg of a catalyst was evenly spread on the side wall of a standard (1 cm optical path, 5 mL volume) rectangular screw cap quartz cell equipped with a teflon/rubber septum. The cell was put in a standard metal holder with its temperature adjusted to 25 °C with a continuous flow of water from a circulating water bath Isotherm 3006 bought from Fisher Company. A gaseous mixture of acetaldehyde in air was passed through the cell until concentration of acetaldehyde was reached about 8 mM. A Gas Chromotograph with a mass selective detector (GCMS-QP5000) from Shimadzu was employed to quantify acetaldehyde and carbon dioxide concentrations. During a typical measurement, acetaldehyde, acetic acid, and carbon dioxide were separated on the column (phase XTI-5, Restek Corp.) maintained at 40 °C. The carbon dioxide and acetaldehyde concentrations were recalculated from the areas under $m/z = 44$ fragment peaks with the use of appropriate calibration curves obtained in separate experiments. The photooxidation of acetaldehyde was carried out under the 546 nm monochromatic irradiation prepared from the light of a 1000 W He(Xe) lamp by passing it through water, neutral density (#59670), and interference (#56561) filters (all from Oriel Instruments). The intensity reaching the powder samples was about 7.4×10^{16} photon s^{-1} cm^{-2} as measured with a Power Max 500D laser power meter from Molectron Detector, Inc. The beam cross section was close to 1 cm^2.

2.4. EPR experiments

X-band EPR measurements were carried out on a Bruker EMX 10/12 spectrometer equipped with an ER 4102 ST standard rectangular resonant cavity in the TE_{102} mode. In a typical experiment, the powdered sample was placed in a suprasil glass tube connected to a high vacuum system. The samples were initially treated at $T = 600$ °C and $p < 10^{-6}$ mbar in order to dehydroxylate the surface. Traces of organic compounds were removed by the treatment at $T = 600$ °C in the presence of 20 mbar O_2. All EPR measurements were carried out at 77 K and residual pressures below 10^{-6} mbar. Irradiation of the samples was carried out with the light of a 300 W Xe lamp (Oriel) being passed through appropriate filters. Reaching the sample light intensity of UV irradiation ($200\text{ nm} < \lambda < 387$ nm) was about 0.7 mW cm^{-2} as measured with a bolometer (International Light). To prepare vis light, the UV and infrared portions of the spectrum of the 300 W Xe lamp were cut off with a 495 nm and water cut off filters.

3. Results

The phase composition of the original TiO_2 P25 from Degussa Corp. is well known and consists of a mixture of anatase and rutile with some amounts of amorphous phase. In a general agreement with literature data, the treatment of TiO_2 Degussa P25 in oxygen at a temperature as high as 800 °C leads to the most thermodynamically stable rutile phase. Thus prepared rutile-TiO_2 was designated as sample A with its XRD pattern shown in Fig. 1. Sample A was later used for further reduction–oxidation treatments. To reach a considerable degree of reduction, the reduction step had to be carried out at high temperatures. As it is clear from the XRD patterns of the reduced titanium oxides presented in Fig. 2, a considerable bulk reduction of rutile starts when the maximal reduction temperature exceeds 1000 °C. Comparison of the recorded patterns with available reference data (showed for Ti_5O_9 and Ti_4O_7 phases) allowed

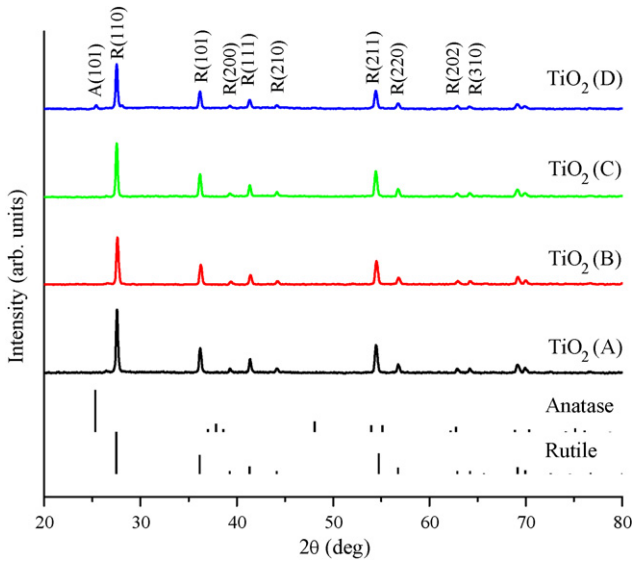

Fig. 1. XRD patterns of the titanium dioxides prepared through different preparation procedures. Sample A was prepared via an 800 °C treatment of Degussa P25 in oxygen. Samples B–D were prepared from sample A via 1000, 1100, and 1180 °C reduction in the flow of hydrogen/argon mixture followed by 800 °C reoxidation in oxygen. All temperatures specified here were the maximal temperatures employed (for details please see Section 2). The reference patterns of anatase and rutile are given for comparison.

us to identify the samples formed after the reduction at maximal temperatures of 1000, 1100 and 1180 °C as being the mixtures of Ti_6O_{11}/Ti_9O_{17}, Ti_4O_7/Ti_5O_9 and Ti_3O_5/Ti_4O_7 correspondingly.

Reoxidation of the reduced titanium oxides in the flow of oxygen results in their conversion back into rutile dominant titanium dioxides (Fig. 1). The samples prepared from Ti_6O_{11}/Ti_9O_{17}, Ti_4O_7/Ti_5O_9 and Ti_3O_5/Ti_4O_7 mixtures are designated as samples B–D correspondingly. Comparison of the experimental XRD patterns of these samples with the reference patterns for two most typical crystalline forms of TiO_2 anatase and rutile demonstrates, however, that some trace amounts of anatase are also present in sample D prepared from the most reduced Ti_3O_5/Ti_4O_7 mixture.

An additional verification of the phase composition of the powders comes from the Raman studies presented in Fig. 3. For all samples, two well-developed peaks at 610 cm^{-1} and around 450 cm^{-1} can be unambiguously assigned to rutile vibrations with

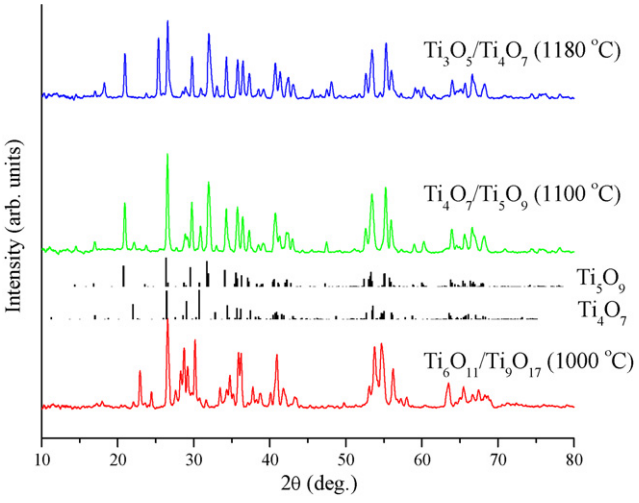

Fig. 2. XRD patterns of the powders formed after reduction of sample A in 4% (v/v) of H_2 in Ar at maximal temperatures of 1000, 1100, 1180 °C. The reference patterns of Ti_5O_9 and Ti_4O_7 are given for the comparison purpose.

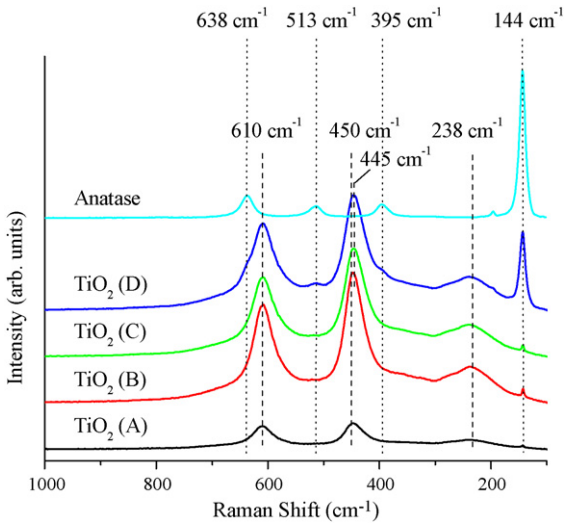

Fig. 3. Raman spectra of samples A–D. The spectrum of a commercial anatase is included as a reference.

A_{1g}, E_g symmetries correspondingly [46]. A well pronounced peak at 238 cm^{-1} was assigned earlier to a non-fundamental combination mode of rutile. Interestingly, all TiO_2 powders exhibit a peak at 144 cm^{-1}. A weak sharp Raman peak at 143 cm^{-1} was observed in a single crystal of rutile and was attributed to B_{1g} vibration. However, the position of this peak coincides with the strongest anatase Raman band at 144 cm^{-1}. Indeed, the Raman spectrum of a reference anatase purchased from Aldrich reveals $E_g(\nu_1)$, $B_{1g}(\nu_2)$–$A_{1g}(\nu_3)$, $B_{1g}(\nu_4)$, $E_g(\nu_5)$ and $E_g(\nu_6)$ bands located at 638, 513, 395, 200 and 144 cm^{-1} correspondingly [47]. Consistently with our XRD observations, the weakly developed bands at 638, 513 and 395 cm^{-1} and the strong band at 144 cm^{-1} show that sample D prepared from the most reduced Ti_3O_5/Ti_4O_7 mixture contains some amount of anatase with rutile to be the dominant phase. As for TiO_2 samples A–C, only a weak peak located at 144 cm^{-1} is observed leaving a possibility that some tiny amounts of anatase undetectable by XRD are still present in these predominantly rutile phase titanium dioxides.

One of the key prerequisites for the appearance of photoactivity in the visible range is an existence of absorption in this region. Consistently with our previous work, an analysis of the UV–vis spectra of the TiO_2 presented in Fig. 4 reveals that the reduction–reoxidation cycle builds an absorption in the visible region. As expected, the value of absorption in the visible region grows with the reduction degree of the samples from which the final TiO_2 were prepared. Indeed, the reoxidation of Ti_6O_{11}/Ti_9O_{17}, Ti_4O_7/Ti_5O_9, and the most reduced Ti_3O_5/Ti_4O_7 yields samples B–D with a progressively higher absorption in the range from 430 to 800 nm.

A well-studied reaction of gaseous acetaldehyde photocatalytic oxidation was employed for probing visible light photoactivities of the prepared titanium dioxides. As seen from Fig. 5, quite consistently with the absorption spectra, the rates of carbon dioxide production under visible ($\lambda = 546$ nm) light increases along with the growth of the absorption in the visible region from sample A to sample D. Blank experiments with the Ti_6O_{11}/Ti_9O_{17}, Ti_4O_7/Ti_5O_9, and Ti_3O_5/Ti_4O_7 powders as well as when no TiO_2 was present showed no detectable rate of the CO_2 formation.

Samples A and C were later chosen for further comparison by means of EPR technique. After dehydroxylation and subsequent oxidation only traces of paramagnetic centers were observed in the EPR spectra at 77 K. These spectra were taken as a reference, whereas the observed difference before and after irradiation is shown in Fig. 6.

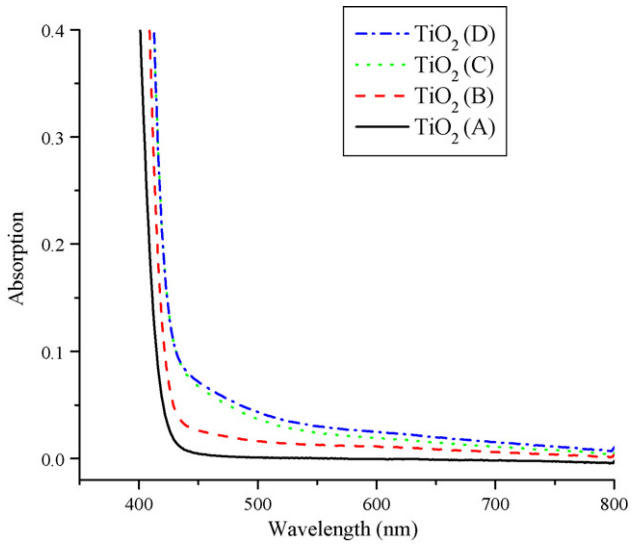

Fig. 4. Optical spectra of samples A–D.

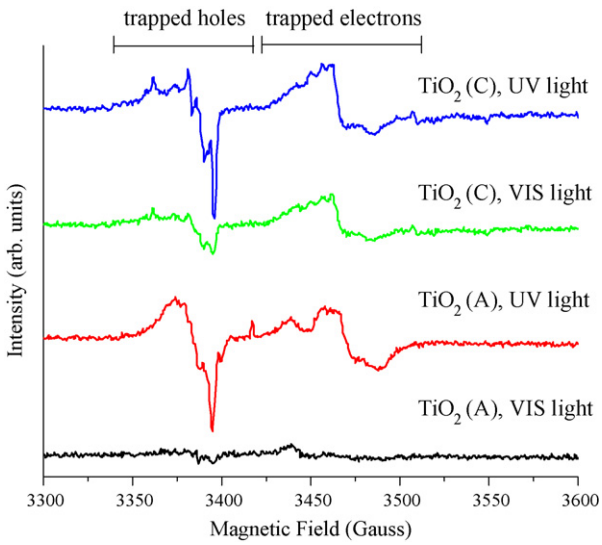

Fig. 6. Difference EPR spectra of TiO_2 (A), TiO_2 (C) samples obtained after UV and vis irradiation, respectively. The spectra right after the thermal activation were used as reference. All measurements were performed at 77 K.

Exposure of visible-light-inactive sample A to the UV light at 77 K induces the formation of paramagnetic centers (Fig. 6). The low field signal can be assigned to holes (h^+) trapped at oxygen ions, $O^{\bullet -}$ [48]. The feature at higher magnetic fields is composed of an axially symmetric signal and has been attributed earlier to trapped electrons on rutile-TiO_2 forming paramagnetic Ti^{3+} centers [49]. A temporary warming (up to 298 K) the samples exposed to UV irradiation at 77 K results in charge carrier recombination and the restoration of the original EPR signal observed before irradiation. As opposite to the UV light, nearly no changes in the EPR spectra are observed when sample A was exposed to vis light ($\lambda > 495$ nm) at 77 K.

Exposure of sample C to the UV light at 77 K again leads to a persistent charge separation. The signal of the trapped electron centers (Ti^{3+}), and more so of the signal for the respective hole centers ($O^{\bullet -}$) look somewhat different from the corresponding signal observed in sample A (Fig. 6). Warming to 298 K once again leads to the restoration of the initial state observed before irradiation. Whereas vis light exposure of sample A nearly does not induce any change in the respective EPR spectrum, a significant degree of charge separation is observed in the case of sample C exposed to the visible light. The variation of EPR signal contours observed on sample C after UV as opposite to the vis exposure lies within experimental margins of error. It precludes us from speculation on possible variation in the nature of the trapping sited involved in capturing charge carries in sample C under UV and vis light.

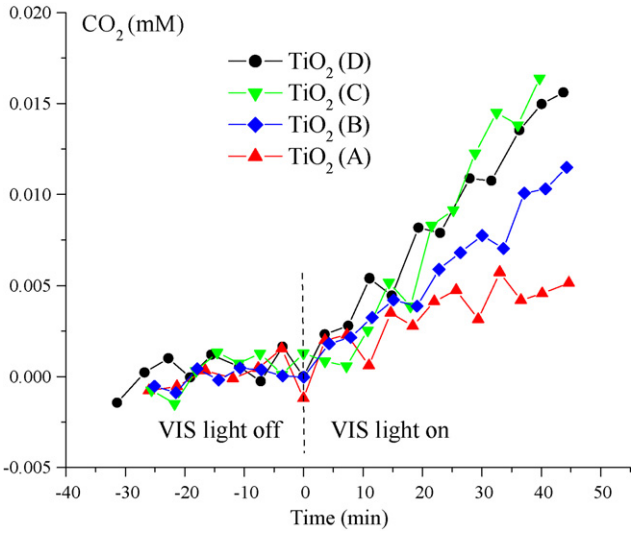

Fig. 5. Evolution of carbon dioxide during photooxidation of gaseous acetaldehyde over samples A–D in air under visible ($\lambda = 546$ nm) light at 296 K.

4. Discussion

Described by Sato et al. [23] and independently rediscovered by Asahi et al. [24] nitrogen-doped titanium dioxides were historically the fist non-metal-doped TiO_2 with a considerable photocatalytic activity in visible light. Since then numerous modifications to the initial preparation recipe has been suggested making preparation of visible-light-active titanium dioxides a relatively simple procedure.

The further research into non-metal-doped TiO_2 revealed that nitrogen was not unique in its ability to bring TiO_2 activity into the visible range. Carbon, sulfur, boron, and iodine could do a similar job. Even more surprising was our finding that the presence of non-metal dopants were not essential to make visible-light-active TiO_2. Indeed, a simple oxidative annealing of TiO or Ti_2O_3 resulted in dopant-free titanium dioxides that not only absorbed a visible part of the spectrum, but demonstrated activities superior to a analogously prepared N-doped TiO_2 [45]. An analysis of the preparation procedures published at this time and our own results led us to speculate about the necessity of the reduction step or the use of titanium compounds already in a reduced state as a common requirement for obtaining visible-light-active titanium dioxides. As a result, the presence of oxygen defects rather than non-metals as such was put forward as the underlying reason for the appearance of visible light absorption and activities in non-metal-doped and dopant-free TiO_2 [45].

Even in our early work [45], the similarity of the visible part of absorption spectra of N-doped, C-doped and dopant-free TiO_2 was quite surprising. Kuznetsov et al. [50] carried out a detailed analysis of the visible part of absorption spectra of titanium dioxides prepared by various means. The authors showed that the similarity goes well beyond a qualitative agreement, but instead is quantitative. The authors argued in favor of oxygen defects as a primary reason for the formation of visible-light-active TiO_2.

The non-metal doping and oxygen defects are not mutually exclusive ideas. For example, as shown in Fig. 7, a simple substi-

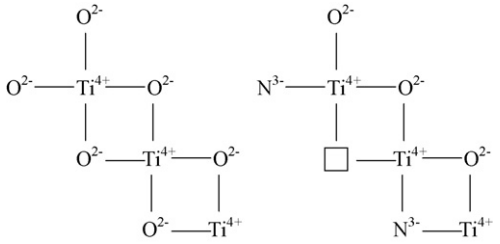

Fig. 7. Formation of oxygen defects upon substitution of oxygen with nitrogen ions in the lattice of TiO_2.

tution of oxygen ions, O^{2-}, with nitride ions, N^{3-}, should lead to the formation of oxygen vacancies in the lattice of TiO_2 to preserve electroneutrality of the sample. The oxygen vacancies, designated in the Fig. 7 by open squares, are also referred to in the literature as $V_O^{\bullet\bullet}$ or F^{2+}-centers. Redistribution of the electron density in the sample may lead to the formation of F-center with one electron in it, F^+, or two electrons in the place of the former oxygen ion, F. The deconvolution of the visible part of optical spectra of visible-light-active titanium dioxides conducted by Emeline et al. [51] revealed an interesting feature: all spectra could be presented as a sum of three bands. Consideration of the experimental data from the point of view of oxygen defects as color centers in conjunction with the available literature data allowed the authors to proceed to a tentative band assignment. In particular, the first two bands of the visible part of the TiO_2 spectra, 413–428 and 477–517 nm were cautiously assigned to Jahn–Teller split of $^2T_2 \rightarrow {}^2E$ transitions of Ti^{3+} centers, whereas the last band 590–729 nm was attributed to the excitation of F^+-center, $F^+ \rightarrow F^{+*}$, or its ionization leading to the formation of conduction band electron, $F^+ \rightarrow F^{2+} + e$.

In this work, we purposely avoided introduction of non-metal ions into the lattice of TiO_2 using just hydrogen for reduction and oxygen for oxidation. Though the high temperatures required to achieve a substantial reduction of the starting TiO_2 resulted in low surface areas (<2 m^2/g) and low photoactivities of final TiO_2 samples, the systematic trend in growing vis light part of the adsorption spectra and visible light activities of the samples is obvious and cannot be related to any non-metal dopants. The EPR technique delivered the same qualitative result reflecting an ability of visible-light-active TiO_2, TiO_2 (C), to generate trapped holes and electrons under vis light and lack of thereof for the reference sample, TiO_2 (A). Though the EPR spectra of trapped holes generated under UV light in TiO_2 (C) and TiO_2 (A) look different (Fig. 6), low signal to noise ratio precluded us from detailed EPR spectra analysis. It is worth noting though, that the trapping sites observed in EPR experiments are not necessarily related to color centers responsible for the appearance of visible light activities in TiO_2. Indeed, giving right circumstances generated at a color center an electron/hole may get detrapped and recaptured by sites, which are higher in energy (for the hole) and lower in energy (for the electron) leading to false interpretation of the result of EPR experimental results.

The hypothesis of a key role of defects in the formation of visible-light-active TiO_2 requires confirmation of oxygen defect existence. Unfortunately, there seems to be not many experimental techniques that can deliver this kind of information. One option available for TiO_2 is Raman spectroscopy. Indeed, Parker et al. reported that for titanium oxides in the region $1.88 < O/Ti < 2.00$, the ratio of oxygen to titanium can be quantitatively assessed by the Raman scattering technique. It was shown, for example, that the position of the Raman peak around 445 cm^{-1} shifts to low wavenumbers as the O/Ti ratio starts to fall. In a recent publication, Wang et al. [52] demonstrated that incorporation of Fe^{3+} into TiO_2 leads to the creation of large amounts of oxygen vacancies, and, as a result, the E_g peak of the rutile located around 447 cm^{-1}

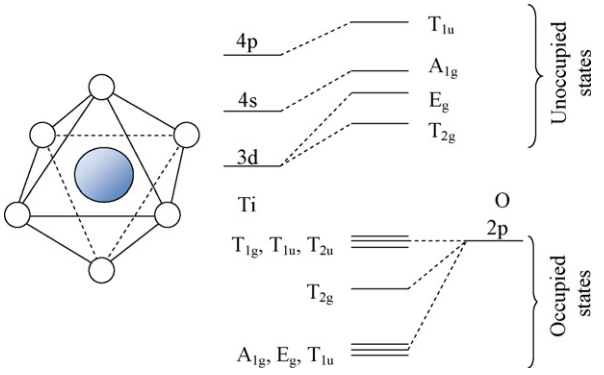

Fig. 8. Titanium ion in the octahedral environment of oxygen ions (left) and a schematic molecular orbital energy diagram of this structure (right).

at zero concentration of iron ions shifts to the low wavenumbers with an increase in iron loading. An analysis of the Raman spectra shown in Fig. 3 confirms that the shift to the low wavenumbers of the E_g peak is unambiguously present but quite small. The difference in the position of E_g peaks for samples A and D remains within 5 cm^{-1} suggesting a slight increase in the number of oxygen defects as we move from a relatively inactive sample A to more active under visible light sample D. The fact that the visible part of absorption spectra (Fig. 4) and the visible light activities of the samples (Fig. 5) remain relatively poorly developed is in accordance with the low quantity of defect sites retained in the employed preparation methods. Indeed, according to the correlation curve measured by Parker, the Ti to O ratios for samples A through D fall within the region $1.99 < O/Ti < 2.00$, suggesting that nearly stoichiometric samples studied in this work.

Apart from the presence of non-metals, or oxygen defects, certain types of concomitant deformations can be conceived as an underlying reason for the appearance of visible light absorption by TiO_2 materials. To elucidate this idea, the following model may be used. The structure of TiO_2 may be envisioned as an arrangement of octahedral building blocks with a titanium ion in the center and six oxygen ions at the vertices. Different TiO_2 polymorphs, rutile, anatase, or brookite can be produced by arranging octahedral blocks in various ways involving oxygen ion sharing [53]. Due to this fact, titanium in the octahedral environment of oxygens is often used as a simple model for generating qualitative predictions about bulk TiO_2 behavior.

The molecular orbital energy level diagram adopted from the publication by Fleming el al. [54] is presented in Fig. 8. 3d, 4s, 4p orbitals of Ti and 2p orbitals of O are included in consideration. An expected energy positions of the orbitals in the TiO_6^{8-} complex are shown in the middle and designated according to their symmetry. Allocation of 36 electrons, zero from Ti^{4+} and 6 from p orbitals of each O^{2-}, results in occupation of low energy TiO_6^{8-} orbitals up to and including T_{1g}, T_{1u}, T_{2u}. Nonbonding linear combinations of O(2p) orbitals of symmetry T_{1g}, T_{1u}, T_{2u} are expected to give rise to the upper part of the valance band, whereas the molecular orbitals of symmetry T_{2g} originated from 3d orbitals of Ti^{4+} with some admixture from 2p orbitals of O^{2-} are expected precursors for the lower part of the conduction band of TiO_2. The energy difference between the highest occupied molecular orbitals (HOMO) and the lowest unoccupied molecular orbital (LUMO) is analogous to the bandgap energy in bulk TiO_2.

As can be seen from this model an elongation of Ti–O bonds should lead to the reduction of energy splitting between LUMO and HOMO. If this elongation to happen for all octahedral blocks in a bulk TiO_2, narrowing of the bandgap is expected. On the other hand, an elongation or deformation of only selective blocks in TiO_2 would result in the formation of point defects that giving right cir-

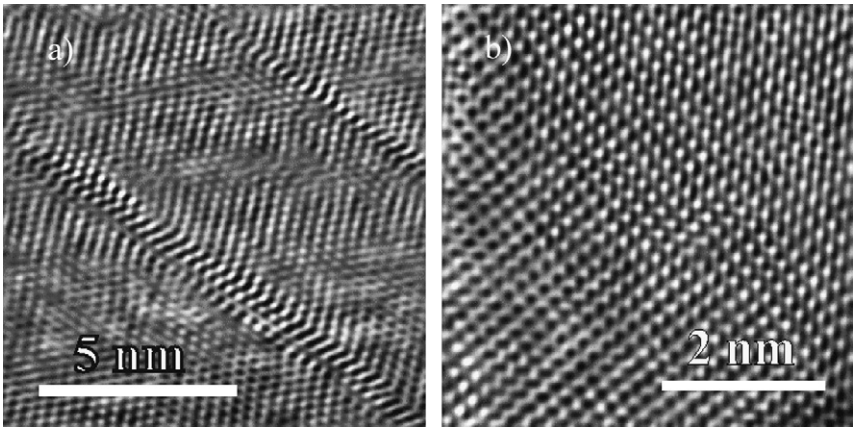

Fig. 9. HRTEM images of the visible-light-active TiO_2 prepared via oxidative annealing of TiO (a) and the visible-light-inactive TiO_2 made though an oxidative annealing of Degussa P25 (b) [45].

cumstances could represent new color centers responsible for the visible light absorption.

Finding of an experimental evidence of an existence of local deformations in the TiO_2 can be a daunting task. In this regard, a difference in structures of the visible-light-active and visible-light-inactive titanium dioxides observed early by us with HRTEM was quite revealing and presented in Fig. 9. In particular, HRTEM studies showed that for the visible-light-active TiO_2 prepared from TiO, considerable amounts of extended defects in the form of thick and thin oriented slabs were present. The dislocations were clearly visible in the structure of the rutile. Evidently, these defects contain titanium ions in altered local atomic environment and generate micro distortions of the TiO_2 lattice. Certainly, point defects as atomic vacancies were present in this structure too. The structural origin of this type of defects most likely stems from the layered structure of intermediate Magnelli phases Ti_nO_{2n-1} consisting of rutile blocks which are infinite in two dimensions and finite in the third [55,56]. Note, that even at low average concentration, point defects organized in such a way are situated quite close to each other and form nice channels to deliver visible light generated charge carries to the surface of TiO_2. In contrast to the visible-light-active TiO_2, an analogous HRTEM study of the visible-light-inactive TiO_2 revealed a nearly perfect lattice structure underlying the importance of defects in the formation of visible-light-active titanium dioxides.

5. Conclusions

In this work the changes to TiO_2 associated with the reduction–oxidation cycles have been studied. In particular, it has been found that the visible-light-inactive rutile titanium dioxides can be activated to the visible light through the high temperature reduction in hydrogen to suboxides Ti_nO_{2n-1} followed by their reoxidation back to rutile-TiO_2. Though the activities under visible light of thus prepared titanium dioxides remain low due low surface areas and small amounts of color centers retained, the preparation procedure does not involve non-metals or transition metal cations traditionally used for this purpose. Instead, the visible light activity likely originates from oxygen defects introduced through the reduction–oxidation cycle. The hypothesis of accumulation of oxygen defects is in line with the Raman studies showing the shift of the E_g band to lower wavenumbers for visible-light-active titania samples. The oxygen defects are likely to be associated with other structural irregularities that may be a contributing factor to the activation of TiO_2 to visible light.

Acknowledgments

The financial support of the Austrian Science Foundation (FWF project P17514-N11) and the Army Research Office through DARPA funded MURI grant (DAAD 19-01-10619) is acknowledged with gratitude.

References

[1] A. Fujishima, K. Honda, Nature 238 (1972) 37.
[2] E.P. Reddy, B. Sun, P.G. Smirniotis, J. Phys. Chem. B 108 (2004) 17198.
[3] S. Rodrigues, S. Uma, I.N. Martyanov, K.J. Klabunde, J. Photochem. Photobiol. 165 (2004) 51.
[4] N. Kakuta, N. Goto, H. Ohkita, T. Mizushima, J. Phys. Chem. B 103 (1999) 5917.
[5] S. Rodrigues, S. Uma, I.N. Martyanov, K.J. Klabunde, J. Catal. 233 (2005) 405.
[6] H. Yamashita, K. Yoshizawa, M. Ariyuki, S. Higashimoto, M. Anpo, M. Che, Chem. Commun. (2001) 435.
[7] S. Rodrigues, K.T. Ranjit, S. Uma, I.N. Martyanov, K.J. Klabunde, Adv. Mater. 17 (2005) 2467.
[8] M. Matsuoka, M. Anpo, J. Photochem. Photobiol. C: Photochem. Rev. 3 (2003) 225.
[9] J. Tang, Z. Zou, J. Ye, Chem. Mater. 16 (2004) 1644.
[10] Z. Zou, J. Ye, K. Sayama, H. Arakawa, Nature 414 (2001) 625.
[11] H. Yoshida, C. Murata, T. Hattori, J. Catal. 194 (2000) 364.
[12] J. Wang, S. Uma, K.J. Klabunde, Appl. Catal. B: Environ. 48 (2004) 151.
[13] A. Hagfeldt, M. Graetzel, Chem. Rev. 95 (1995) 49.
[14] A.L. Linsebigler, G. Lu, J.T. Yates, Chem. Rev. 95 (1995) 735.
[15] O. Legrini, E. Oliveros, A.M. Braun, Chem. Rev. 93 (1993) 671.
[16] P.V. Kamat, Chem. Rev. 93 (1993) 267.
[17] M.A. Fox, M.T. Dulay, Chem. Rev. 93 (1993) 341.
[18] M.R. Hoffmann, S.T. Martin, W. Choi, D.W. Bahnemann, Chem. Rev. 95 (1995) 69.
[19] A. Fujishima, T.N. Rao, D.A. Tryk, J. Photochem. Photobiol. C: Photochem. Rev 1 (2000) 1.
[20] M. Anpo, Res. Chem. Intermediates 11 (1989) 67.
[21] W. Choi, A. Termin, M.R. Hoffmann, J. Phys. Chem. 98 (1994) 13669.
[22] H. Yamashita, Y. Ichihashi, M. Takeuchi, S. Kishiguchi, M. Anpo, J. Synchrotron Rad. 6 (1999) 451.
[23] S. Sato, Chem. Phys. Lett. 123 (1986) 126.
[24] R. Asahi, T. Morikawa, T. Ohwaki, K. Aoki, Y. Taga, Science 293 (2001) 269.
[25] H. Irie, Y. Watanabe, K. Hashimoto, J. Phys. Chem. B 107 (2003) 5483.
[26] J.L. Gole, J.D. Stout, C. Burda, Y. Lou, X. Chen, J. Phys. Chem. B 108 (2004) 1230.
[27] S. Sakthivel, M. Janczarek, H. Kisch, J. Phys. Chem. B 108 (2004) 19384.
[28] C.W.H. Dunnill, Z.A. Aiken, J. Pratten, M. Wilson, D.J. Morgan, I.P. Parkin, J. Photochem. Photobiol. A: Chem. 207 (2009) 244.
[29] S.U.M. Khan, M. Al-Shahry, W.B. Ingler Jr., Science 297 (2002) 2243.
[30] S. Sakthivel, H. Kisch, Angew. Chem., Int. Ed. 42 (2003) 4908.
[31] H. Irie, Y. Watanabe, K. Hashimoto, Chem. Lett. 32 (8) (2003) 772.
[32] Y. Choi, T. Umebayashi, S. Yamamoto, S. Tanaka, J. Mater. Sci. Lett. 22 (2003) 1209.
[33] C.W. Dunnill, Z.A. Aiken, A. Kafizas, J. Pratten, M. Wilson, D.J. Morgan, I.P. Parkin, J. Mater. Chem. 19 (2009) 8747.
[34] T. Ohno, T. Mitsui, M. Matsumura, Chem. Lett. 32 (4) (2003) 364.
[35] T. Umebayashi, T. Yamaki, S. Tanaka, K. Asai, Chem. Lett. 32 (4) (2003) 330.
[36] W. Zhao, W. Ma, C. Chen, J. Zhao, Z. Shuai, J. Am. Chem. Soc. 126 (15) (2004) 4782.
[37] W. Su, Y. Zhang, Z. Li, L. Wu, X. Wang, J. Li, X. Fu, Langmuir 24 (2008) 3422.

[38] O. Diwald, T.L. Thompson, E.G. Goralski, S.D. Walck, J.T. Yates, J. Phys. Chem. B 108 (2004) 52.
[39] O. Diwald, T.L. Thompson, T. Zubkov, E.G. Goralski, S.D. Walck, J.T. Yates, J. Phys. Chem. B 108 (2004) 6004.
[40] C.D. Valentin, G. Pacchioni, A. Selloni, Phys. Rev. B 70 (2004) 085116.
[41] C.D. Valentin, G. Pacchioni, A. Selloni, Chem. Mater. 17 (2005) 6656.
[42] C.D. Valentin, G. Pacchioni, A. Selloni, S. Livraghi, E. Giamello, J. Phys. Chem. B 109 (2005) 11414.
[43] T. Ihara, M. Miyoshi, M. Ando, S. Sugihara, Y. Iriyama, J. Mater. Sci. 36 (2001) 4201.
[44] I. Nakamura, N. Negishi, S. Kutsuna, T. Ihara, S. Sugihara, K. Takeuchi, J. Mol. Catal. A 161 (2000) 205.
[45] I.N. Martyanov, S. Uma, S. Rodrigues, K.J. Klabunde, Chem. Commun. (2004) 2476.
[46] S.P.S. Porto, P.A. Fleury, T.C. Damen, Phys. Rev. 154 (1967) 522.
[47] T. Ohsaka, F. Izumi, Y. Fujiki, J. Raman Spectrosc. 7 (6) (1978) 321.
[48] R.F. Howe, M. Grätzel, J. Phys. Chem. 91 (1987) 3906.
[49] D.C. Hurum, A.G. Agrios, K.A. Gray, T. Rajh, M.C. Thurnauer, J. Phys. Chem. B 107 (2003) 4545.
[50] V.N. Kuznetsov, N. Serpone, J. Phys. Chem. B 110 (2006) 25203.
[51] A.V. Emeline, V.N. Kuznetsov, V.K. Rybchuk, N. Serpone, Int. J. Photoenergy (2008) 258394.
[52] X.H. Wang, J.-G. Li, H. Kamiyama, M. Katada, N. Ohashi, Y. Moriyoshi, T. Ishigaki, J. Am. Chem. Soc. 127 (2005) 10982.
[53] A. Beltran, L. Gracia, J. Andres, J. Phys. Chem. B 110 (2006) 23417.
[54] L. Fleming, C.C. Fulton, G. Lucovsky, J.E. Rowe, M.D. Ulrich, J. Luning, J. Appl. Phys. 102 (2007) 033707.
[55] M. Reece, R. Morrell, J. Mater. Sci. 26 (1991) 5566.
[56] M. Marezio, D.B. McWhan, P.D. Dernier, J.P. Remeika, Phys. Rev. Lett. 28 (21) (1972) 1390.